# Image analysis of palm oil crystallisation as observed by hot stage microscopy

*Peter D. Harrison[a], Kevin W. Smith[b], Krishnadath Bhaggan[c], Andrew G.F. Stapley*[a]*

[a]Department of Chemical Engineering, Loughborough University, UK.

[b] Fat Science Consulting Ltd, Bedford, UK.

[c] Loders Croklaan B.V., Wormerveer, The Netherlands.

Running title: Image Analysis of Palm Oil Crystallisation

Corresponding author:

Dr Andrew G.F. Stapley

Department of Chemical Engineering,

Loughborough University,

Loughborough,

Leicestershire,

LE11 3TU,

United Kingdom.

Phone: +44-1509-222525.

Email: A.G.F.Stapley@Lboro.ac.uk

**Abstract**

An image processing algorithm previously used to analyse the crystallisation of a pure fat (tripalmitin) has been applied to the crystallisation of a multicomponent natural fat (palm oil). In contrast to tripalmitin, which produced circular crystals with a constant growth rate, palm oil produced speckled crystals caused by the inclusion of entrapped liquid, and growth rates gradually decreased with time. This can be explained by the depletion of crystallisable material in the liquid phase, whereas direct impingement of crystals (the basis of the Avrami equation) was less common. A theoretical analysis combining this depletion with assuming that the growth rate is proportional to the supersaturation of a crystallisable pseudo-component predicted a tanh function variation of radius with time. This was generally able to provide good fits to the growth curves. It was found that growth rate was a relatively mild function of temperature but also varied from crystal to crystal and even between different sides of the same crystal, which may be due to variations in composition within the liquid phase. Nucleation rates were confirmed to vary approximately exponentially with decreasing temperature, resulting in much greater numbers of crystals and a smaller final average crystal size at lower temperatures.

**Keywords:** A1. Crystal morphology; A1. Growth models; A1. Nucleation; A1. Optical microscopy; A2. Growth from melt; B1. Triacylglycerol.

## 1. Introduction

Palm oil is the world's most exported vegetable oil. It is a key component in products ranging from soaps to margarine and is one of the few vegetable oils with high amounts of saturated fats, hence it is semi-solid at room temperature. It is typically fractionated into higher value products for specific applications in foods[1]. It is important to understand how palm oil crystallises with particular reference to palm oil fractionation and palm oil applications, but also in advancing our understanding of the crystallisation of fat systems in general. Previous studies of RBD palm oil crystallisation have employed a variety of techniques including Differential Scanning Calorimetry (DSC)[2-4], light microscopy[5], X-ray Diffractometry (XRD)[6] or a combination of these methods, to build up information of polymorphic behaviour and crystallisation kinetics.

Palm oil is a complex mixture of triacylglycerols (TAGs) which can be seen to crystallise into two distinct populations when slowly cooled in a DSC[3, 5, 7], typically one in the range 30-20 °C ("high melting") and the other below 15 °C ("low melting"). In addition to this, palm oil displays multiple polymorphic forms. The polymorphism of palm oil is most reliably determined from XRD experiments, and is now reasonably well understood. Persmark and co-workers[8], conducting XRD experiments, found the existence of three polymorphs, which were named $\alpha$, $\beta_1'$ and $\beta_2'$. $\beta_1'$ was found when samples were cooled at a slow rate to 22 °C. $\beta_2'$ (which from Persmark's description could actually be a sub- $\alpha$ form) was formed from fast cooling to -15 °C (presumably from "low melting" TAGs), and $\alpha$ and $\beta_1'$ at intermediate conditions. Another study*[9]* also found that small amounts of $\beta$ (affecting only a small proportion of TAGs) could co-exist with $\beta'$, and that both were stable until melted. Some $\beta$ forms were also found at temperatures below 0 °C, which were presumed to be due to the low melting fractions. Isothermal XRD experiments (of particular relevance to this study) were performed by Chen *et al.[10]* from 287 to 295 K. They found that the $\alpha$ form formed initially for T < 20 °C (reported as 293 K) but

transformed to *β'* over time (of the order of 30 min). A "two stage" process was also evident from viscosity vs time experiments. Further experiments using light microscopy showed what appear to be *β'* spherulites growing around an *α* core. As a consequence of this the authors discussed the possibility that XRD data may not always provide a complete picture of the polymorphic state of a sample if a polymorph at the surface is covering over a different polymorph underneath.

The kinetics of palm oil crystallisation have also been studied by a number of workers. Kawamura[2] performed isothermal DSC experiments in the range 299 K to 303 K from which Avrami fits to solid fat content (SFC) vs time data were made. He then used light microscopy to directly determine growth rates at these temperatures, and used the growth rate information to back-calculate nucleation rates from the Avrami fit constants. Ng and Oh[4] performed an Avrami fit over a wider range of temperatures but without additional growth rate measurements. Induction time data have also been determined from DSC[5] and fitted to expressions for nucleation rate although it is questionable to do this as these represent physically distinct phenomena[11].

Recently, a method of analysing hot stage microscope images of crystallisation has been reported[12]. This automates the process by which crystals can be counted and size measurements made so that data from a series of images containing potentially large numbers of crystals can be relatively easily extracted and analysed. The method has so far been applied to tripalmitoyl-glycerol (also known as tripalmitin) which is a pure TAG. The aim of this paper is to test whether the computer based method can be successfully applied to palm oil, and useful information regarding nucleation and growth extracted that may not be apparent by manual methods.

## 2. Materials and methods

### 2.1 Palm oil

Palm oil was obtained from the Malaysian Palm Oil Board and used without further treatment. The composition as determined by HPLC is given in Table 1 using the following method.

### 2.2 Compositional analysis by HPLC

TAG analysis was performed using an HPLC instrumentation system equipped with a Hewlett Packard HPLC binary pump system (model HP 1100 Series, Waldbronn, Germany), a variable loop injector system, a column oven and an Agilent refractive index detector (Agilent 1100 Series, Waldbronn, Germany). TAGs were separated on two identical Waters Nova-Pak© C18 (Waters Corp., Darmstadt, Germany) columns connected in series with column dimensions of 3.9 mm internal diameter by 300 mm length (each) and preloaded with silica with a particle size of 4 μm. Both columns were maintained at a temperature of 25 °C. The mobile phase used was a mixture of HPLC-grade acetone (Fisher Scientific, Loughborough, UK) and HPLC-grade acetonitrile (Fisher Scientific, Loughborough, UK) in a volume-to-volume (v/v%) ratio of 63.5:36.5 and the flow-rate was fixed at 1 mL/min. The injection volume was set to 10 μL of 5% (w/v) of oil in chloroform. Attenuation was fixed at 500 x 103 RI units and the refractive index detector was maintained at 35 °C. The total runtime for a single injection was 130 min. Identification of TAGs was made based on the retention time of TAG standards and by comparison with the literature. Peak integrations were carried out using the HPLC ChemStation integration software. Integrated peak areas of TAGs and other minor components were normalised based on the total area of all peaks present in the chromatogram. Other minor components such as MAGs and DAGs were not quantified individually and their concentrations were collocated together and their total concentration expressed as ‘Others’. HPLC results were expressed in weight percentages (wt%)[13].

### 2.3 Hot stage microscopy

Optical microscopy experiments were carried out using a Linkam THMS600 variable temperature stage (Linkam Instruments, Tadworth, UK) with a Leitz (Diaplan) microscope coupled to a PixeLink PL-A662 digital camera (PixeLink, Ottawa, Canada) and Linksys 32 software data capture system (Linkam Instruments, Tadworth, UK).

The palm oil was first heated to 70 °C, and a small sample was then weighed on to a circular glass slide which was positioned on a hot plate at approximately 70 °C. Another cover slip was then placed concentrically on top of the drop to ensure a uniform thickness of the sample. A photograph was then taken of each slide which was taken at such an angle as to clearly show all the oil on the slide. From this, the area of the palm oil sample was calculated by counting pixels (using image analysis) and using the known area of the glass cover slip as a reference to convert pixels to area. Such an approach allowed photographs taken at an oblique angle to also be used as the angle would affect the view factors of the cover-slip and the oil equally. The area of the oil combined with the mass of oil weighed on to the slide and an assumed density of 922 kg $m^{-3}$ enabled the thickness of the oil sample to be estimated. The sample was subsequently placed in the temperature stage, where it was heated to 70 °C and held for a minimum of 3 min. Thereafter the sample was cooled at a rate of 30 °C $min^{-1}$ to an isothermal holding temperature. Fast cooling was achieved by passing liquid nitrogen through the stage. Images (1280 x 1024 pixels) were collected during the isothermal holding period, observed via a 10× objective lens and captured automatically every 30-60 s (depending on the temperature and holding period) using Linksys software. The images were scaled by taking an image of a graticule at the same magnification. The temperature was held at the isothermal holding temperature until no further changes were easily discernible. Samples were then heated at 1 °C.$min^{-1}$ to ~70 °C to allow melting or polymorphic transformations to be visualised and held for 3 minutes before once again cooling to another isothermal temperature.

In the case of holding at 35 °C it was found that crystallisation was possible within approximately 4 h, but that only a few crystals would have formed over the entirety of the slide. A number of attempts were made to catch the initial nucleation event but these were unsuccessful due to the very low probability of viewing the relevant area of the slide as the nucleation event occurs (only ~1/100th of the total slide area is visible under the microscope at any one time). Therefore, while the morphologies of these crystals can be reported, the nucleation and growth data are not.

### 2.4 Image analysis

All image analyses were performed in MATLAB (The Mathworks Inc, Natick, MA) using routines from the Image Processing Toolbox, based on the method employed for tripalmitin crystallisation[12]. Some modifications to the method were made in response to the different morphologies observed in the crystallisation of tripalmitin and palm oil. Analyses were performed for experiments with isothermal hold temperatures of 23 °C or higher. Temperatures below this were not analysed as crystals started nucleating before isothermal conditions were reached.

In contrast to tripalmitin, palm oil produced crystals with a speckled appearance which made it more difficult for the algorithm to distinguish newly nucleated crystals against the background noise as no one single speck would generally be sufficiently large by itself to reliably indicate a new crystal. However, a cluster of speckles was usually obvious by eye (see the cluster in e.g. Figure 1a). Thus a different approach for nucleation detection was adopted which would be sensitive to the formation of clusters of “specks”. A transform was employed by which the number of non-zero pixels within a square (of 21 pixels x 21 pixels) centred on a given pixel was returned for that pixel. This was performed for each pixel in the image and effectively returns a local “density” map of non-zero pixel counts within the immediate vicinity of a pixel (see Figure 1b). Then when the number of non-zero pixels in the 21x21 square exceeds a threshold value (Figure 1c) this triggers a “nucleation” in the

crystalmap which is located at the maximum density pixel of the cluster (Figure 1d). This method was found to provide a more robust method for nucleation detection.

A second modification arose from finding that the red, green and blue colours responded differently to the presence of a crystal speck. Whereas the red and blue components of the images were made darker by the presence of a crystal, the blue component appeared brighter. Thus to give greater contrast, grayscale images were produced not from adding the red, green and blue components together but by adding the red and green components and subtracting the blue.

An example of the running of the algorithm is shown in Figure 2. Figure 2a shows the raw image (the contrast of which has been artificially enhanced for publication purposes). The crystals in the image are “speckly” in nature (see Figure 2a) and running the algorithm produces a corresponding “speckly” crystalmap (Figure 2b). The coloured (non-black) regions can be thought of as approximately representing the amount of solid in the crystals. To quantify the amount of space occupied by a crystal (including entrained liquid) the internal cavities within the crystalmap need to be filled in. This can be achieved using the MATLAB dilation/erosion routine, “imclose.m”. In this method each crystal is taken on its own and grown by a certain number of pixels (in our case we chose 10 pixels). This would dilate (grow) the outer boundary but also the internal boundaries which should grow into each other and disappear. The expanded boundaries would then be eroded back by the same amount (10 pixels), which restores the exterior boundary to its original position with some minor smoothing, but will have filled in interior holes and exterior cracks. This produces a “filled map” (see Figure 2c). This map is used for the majority of subsequent calculations (such as growth rate and crystal size). It was also decided to use the “unfilled” maps (e.g. Figure 2b) to also estimate the actual solid fat content by counting only the unfilled pixels. However, the “unfilled” maps generally became corrupted with noise pixels over the course of adding dozens of images, so a “clean” version of the unfilled map was

produced. This was obtained by subtracting the current image from the very first image of the run, thresholding the result to produce a binary map of current pixels and then using this as a mask over the filled map to produce the new “clean” version (see Figure 2d). It can be seen that this is a better representation of the crystals in Figure 2a than Figure 2b.

A fourth issue relates to the measurement of crystal radii for growth rate studies. The method used for tripalmitin[12] took the average radial position of all new growth pixels added with each new image. This worked well for tripalmitin which displayed approximately constant growth rates. However, as will be shown later, palm oil crystals’ growth slows down with time until almost no growth is observed. At this point very few, if any, growth pixels are observed and the radial average values become more influenced by noise pixels. Instead, the radius was evaluated as the average radius of the furthermost pixels from the centre, the number of which was determined as that which would form a bilayer of pixels at the circumference if the crystal were completely circular (a bilayer gave more reliable results than a monolayer). This was performed using the “filled” crystalmaps e.g. Figure 2c. The resulting radial values are shown graphically in Figure 2e. It can be seen that, in many cases, the crystals do not form perfect circles. Overlapping circles are caused by crystals nucleating close to one another and growing into each other.

## 3. Results and discussion

### 3.1 Crystal morphology and polymorphism

Example images from the crystallisation of palm oil at various temperatures in the range 20 - 35 °C are shown in Figure 3. Very well defined spherulites are observed at 32 °C and 35 °C, but crystals are more speckled at lower isothermal temperatures (down to 26 °C). The spherulitic/needle morphologies were also observed by Kawamura[2] at 30 °C (who tentatively ascribed them to the *β* polymorph) and Chen *et al.[10]* at 28 °C. Chen *et al*., however, identified such crystals as belonging to the *β’* polymorph using XRD. At the lower temperatures of 20 and 22 °C a different morphology (reminiscent of the appearance of

coffee beans) is seen, which can be attributed to the *α* polymorph (again following Chen *et al.*). At 24 °C an intermediate morphology is observed, which was also observed by Chen *et al.* who interpreted this as based on an *α* core surrounded by a *β'* exterior. This is borne out by watching the time evolution of experiments at 24 °C in Figure 4. After 10 min of isothermal hold (Figure 4a) a mixture of *α* and *β'* crystals can be seen. After further holding (Figure 4b and 4c) some "speckly" growth is seen around all crystals. However, as the temperature is raised after the end of the isothermal hold (Figs 4d-h) the outer regions of the crystals gradually melt first (completely melting by 42 °C) leaving the cores to melt finally around 45-48 °C (the 35 °C sample finishing melting at 48 °C). These core melting temperatures do not correspond to the melting of the *α* polymorph and so these crystal cores must have transformed from *α* to either the *β'* or *β* polymorph during holding and/or melting. It is well established from XRD studies that polymorphic transitions readily occur from the *α* form under such conditions. However, a possible drawback of XRD is that it may only observe the surface polymorphism of crystals which may well differ from a core polymorph hidden below the surface.

When crystals formed at temperatures in the range 26 - 35 °C were gradually warmed, they gradually reduced in size. This might suggest that the composition of the crystal changes with radial position in the crystal (with higher melting TAGs towards the centre), but it can also be explained by a general increase in solubility with temperature. All crystals were found to finally melt at temperatures above 42 °C (see Table 2), indicating that polymorphic transformations occurred in all cases.

The speckled nature of all the crystals is in sharp contrast to that seen during tripalmitin crystallisation, where well formed circular crystals were formed with no internal cavities[12]. This is a consequence of crystallising from a pure melt. With palm oil at these temperatures a significant "low melting" fraction exists which is unable to crystallise and must diffuse away from the interface. It is apparent from the morphologies produced that

much of this uncrystallisable “solvent” fraction is unable to diffuse away fast enough to avoid becoming trapped by crystal growth around it – giving rise to the speckly morphology. In the microscope slide environment there are likely to be few convection currents and so mass transfer would be almost purely by diffusion. The situation, however, is likely to be different in a stirred tank or other flow environment where the “solvent” molecules may have a better chance to be transported away from the crystal surface before becoming entrapped.

The non-circular nature of some crystals (see Figure 2d) also suggests that non-uniformities in composition of the liquid phase arise due to differences in the extent of crystallisation locally, giving different growth rates in different directions. So the liquid phase cannot be considered to be fully mixed in these experiments.

### 3.2 Solid fat content

The fractional coverage of images from all crystals vs time is shown in Figure 5a for filled (e.g. Figure 2c) and in Figure 5b for clean, unfilled (e.g. Figure 2d) crystalmaps. The fractional coverage of unfilled crystalmaps can be argued to approximately represent the solid fat content of the samples. They produce the “s-shaped” curve typically found on SFC vs time plots with the final (equilibrium) coverage increasing with decreasing temperature. These are similar in form to published SFC vs time plots obtained from DSC data[4], and the final values for the unfilled crystalmaps at 25 °C (the only directly comparable temperature) are also similar. However, the interaction of light with the crystals is not well known and so the precise edge (and therefore thresholding point that should be used when creating the clean crystalmaps) of the crystallites is not known exactly. This is more of an issue with the speckly crystals found with palm oil (compared with tripalmitin) as there is a much larger interfacial area between the liquid and solid phases. Consequently the thresholding value used to create Figure 2d has a significant

effect on the SFC values obtained. In this case the thresholding value used was chosen by eye to match the original images most closely and the same value was used for all runs.

There was a general trend of increasing SFC with lower isothermal hold temperature, which is well established for fat systems and arises from a greater proportion of the TAG molecules being able to crystallise at the lower temperatures. However, there was an anomalous result for 26 and 27 °C which did not follow this order. This is probably due to the low number of crystals observed on the 26 °C experiment (see later nucleation data). This is a hazard of the microscope technique which only samples a small number of crystals (as opposed to DSC and pNMR) and so is open to some statistical variation. However, the data obtained are still useful, for example the experimental data from 23 °C clearly show evidence for two separate processes taking place, which arise from the formation of the two different polymorphs.

### 3.3 Nucleation data

The number of crystals on each image is plotted vs time on Figure 6a. The instantaneous slope of each line is proportional to the nucleation rate. To allow for the fact that nucleation cannot take place in already existing crystals, a second plot is shown of number of crystals vs a modified time variable defined:

$$t_{\mathrm{mod}} = \int_{t_{ind}}^{t} X_L \, dt \qquad (1)$$

where $X_L$ is the fractional liquid coverage. The reader is directed to Stapley *et al.* (2009) for the derivation of this variable. Here, a choice needs to be made between using unfilled or filled crystalmaps for evaluating the fractional liquid coverage. We have chosen to use the filled crystalmaps based on the principle that nucleation of a new crystal is impossible within a filled region.

Both Figure 6a and 6b show evidence of two nucleation processes taking place (one for each polymorph). It should also be noted that nucleation rates, whilst being reasonably

constant over the initial part of each experiment, do reduce towards zero over time as equilibrium conditions are reached. Initial nucleation rates can be calculated from the initial slopes of each graph and are presented in two ways: (i) calculated per unit volume of liquid in each image (this requires measured sample thicknesses, see section 2.2), and (ii) calculated per unit area of sample in each image. The results are presented in Figure 7 and Table 2 and show an approximately exponential variation with temperature, giving rise to the much larger numbers of crystals present at the lower temperatures. There is a more consistent trend observed with the "per unit area" graph (Fig 7(b)), which arises from differences in measured sample thicknesses between temperatures. This suggests that the nucleation events scale with the area rather than volume, and thus is triggered by nucleation sites on the glass slides. Table 2 also shows nucleation data obtained by Kawamura[2]. These are an order of magnitude lower than reported here. However, it should be borne in mind that Kawamura's data are back-calculated from a DSC/Avrami analysis, which is a completely different method to that used here.

Induction times can also be deduced from the point where the number of crystals first rises above zero in Figure 6a and are also presented in Table 2. A similar discontinuity with temperature to that seen by Chen *et al.*[10] is observed. They suggested that the discontinuity observed in the induction data was caused by a change in the polymorphic forms present and that below temperatures of 298 K two palm oil polymorphs, *α* and *β'* crystallised separately.

### 3.4 Growth data

Plots of crystal radii vs time are shown in Figure 8 a, b, c and d for holding at 23, 26, 29 and 32 °C respectively. For 23 °C only crystal data from the central third of the image in both x and y directions (i.e. one ninth of the image area) are shown, for clarity. All data sets show the growth rates of each crystal gradually declining over time, as crystallisable material is consumed from the liquid melt. This is in stark contrast to the constant growth

rates observed with tripalmitin[12]. It also highlights a flaw in the Avrami analysis assumptions for SFC vs time data for palm oil crystallisation, which assumes a constant growth rate. Whereas the Avrami analysis models the reduction in liquid-to-solid transformation rate as an impingement effect, for palm oil (and probably other natural fats) it is actually caused by a reduction in growth and nucleation rates. The radius plots shown in Figure 8 show that there are also noticeable variations in growth rate, probably due to variations in liquid compositions surrounding each crystal. This follows on from the observation made from Figure 2d, which showed that growth rates can vary even on different sides of the same crystal.

To characterise and compare growth rates it was decided to focus on measuring initial growth rates of each crystal. Three methods were used:

(i) A straight line fit over the initial period of growth up to 30% of the final crystal size (during this period the growth was adjudged to be reasonably linear before tailing off).

(ii) A fit to a curve of the form $r = r_f.tanh\big(b(t - t_0)\big)$ (2)

(iii) A fit to a curve of the form $r = r_f.\Big(1 - exp\big(-b(t - t_0)\big)\Big)$ (3)

The tanh expression has some theoretical basis, and a derivation of the equation is shown in Appendix A. Palm oil is a complex multicomponent mixture, but for simplicity the derivation considers the palm oil to be divided into two “pseudo-components”: (i) a crystallisable component, and (ii) a non-crystallisable liquid “solvent”. The growth rate is assumed to be proportional to the supersaturation of the crystallisable component (although in practice a simple concentration driving force produces the same functional form and this assumption is used in the derivation). As a crystal grows, it consumes the crystallisable component from a fixed volume of liquid phase surrounding it which reduces in concentration (via a mass balance), and hence reduces the growth rate.

The latter two expressions were fitted over the whole of the growth curve for each crystal to determine the fit parameters, $r_f$, $b$ and $t_0$. In both cases, $r_f$ represents the final crystal size, $b$ a kinetic constant (numerically different for each model) and $t_0$ the time at which nucleation occurs. The initial growth rate (at $t = t_0$) is given by $r_f \times b$ (the same expression applies for both cases).

Fits to a representative curve for each temperature (the first to nucleate) are shown in Figs. 9 a, b. Given that the growth curves did show some fluctuations in places, the equations generally fitted the data well, particularly at the higher temperatures. At lower temperatures (particularly 23 °C), the curves sometimes did not fit the earliest data points very well. This is attributed to polymorphism, as initially the *α* form grows relatively quickly but this then gives way to a slower growing *β'* form. It is perhaps unrealistic to expect such a change in kinetics to be captured by the single equation, unless it is fitted in a piecewise fashion over single polymorph ranges. A later curve from 23 °C is also shown on Figure 9a and clearly shows an initial jump (due to the *α* polymorph growth), which is again not captured by tanh or exponential equations. It can be seen that the gradient of this jump is similar to the gradient of the straight line fit from the earlier curve at 23 °C.

The fitted growth data are shown in Table 2 and Figure 10. These are the average and standard deviations of fits to crystals that ultimately grow larger than 15 μm in radius. Also shown in brackets are the averages of the RMS error values for each fit type. The following observations can be made:

1. The error bars (standard deviations) are quite large in relation to the average growth rates, and reflects the inherent variability of growth rates between crystals.
2. The different fit expressions gave different results, with linear fits generally giving the lowest values and exponential fits the highest values. There is a tendency for linear fits to underestimate growth rates as they do not represent the very initial growth period

(i.e. a tangent to the growth curve at nucleation), but rather an average growth rate over a period where there will be some reduction (if small) of growth rate. On the other hand, visual inspection showed the tanh and exponential functions to sometimes overestimate initial growth rates on some occasions.

3. The tanh curves overall tend to give better fits than the exponential curves, judging by the lower RMS error values. They also yielded smaller standard deviations. The linear fits gave the smallest RMS values but it should be recognised that these are only based on a small part of the data and not the whole curve.

4. The variation with temperature appears relatively modest and is within the range of the error bars. There are two exceptions: 32 °C which gave much smaller growth rates than other temperatures, and 23 °C in which the linear fit (*α* polymorph) gave a much higher value.

5. Growth rates were approximately half those reported by Kawamura[2]. There may be two reasons for this. Firstly, a manual method used by Kawamura may have naturally selected the fastest growing crystals. Secondly, the palm oil itself may be different in composition. So it is possible that the Kawamura sample may have had, for example, a higher tripalmitin content, which could have led to higher growth rates and nucleation at higher temperatures.

### 3.5 Crystal size distributions

The automated analysis allows a calculation of crystal size distributions which are presented in Figure 11 for the endpoint of each isothermal hold. This clearly shows the general trend of smaller average crystal size as temperatures are reduced which is a consequence of the faster nucleation rates relative to growth rates.

## 4. Conclusions

This study has successfully demonstrated that it is possible to extract nucleation and growth rate data from a series of light microscope images showing crystallisation of the natural fat palm oil. This used an image processing algorithm adapted from that used on the pure fat tripalmitin[12]. The amount of potentially crystallisable material can be judged from final values of solid fat content which can be calculated from “unfilled” crystalmaps, although this is not a precise determination. The speckled nature of the *β’* crystals suggests that uncrystallisable material is not able to diffuse away fast enough from the crystal surface to avoid becoming entrapped within the crystal as it grows around it.

A strength of the microscopy technique is the ability to view the morphology of crystals, which in some cases appear to consist of a mixture of polymorphs (e.g. at 23 °C, 24 °C and 25 °C) with an *α* core and a *β’* exterior. However, the *α* core must then transform to a higher polymorph at some point as it melts at similar temperatures to other *β’* crystals. As mentioned by Chen *et al.*[10], this type of observation may not be observable by XRD which mostly probes the surface regions of crystals.

From growth curves, it can be seen that there are variations of growth rate between crystals at a given time and between different sides of the same crystal, which may be a consequence of imperfect mixing within the melt. This is not altogether unsurprising given that the only mechanism of mixing in this system is likely to be molecular diffusion. It was also observed that the growth rate of a crystal slows during crystallisation, which is a consequence of the depletion of crystallisable matter as time proceeds. A theoretical analysis of the growth curves was performed assuming that growth rates are proportional to the supersaturation of a crystallisable pseudo-component from a fixed volume of a well mixed pool of liquid surrounding each crystal. This predicted a tanh function variation of radius with time, which was able to provide good fits to most data. The main exceptions were at lower temperatures (e.g. 23 °C), which showed an initially fast period of growth,

corresponding to growth of the *α* polymorph, followed by slower growth of the *β'* polymorph. Apart from that, and the very highest temperature (32 °C), it appeared that growth rates were relatively insensitive to temperature, which was in contrast to nucleation rates which were a strong function of temperature.

**Acknowledgement**

We would like to thank Dr. Bill MacNaughtan, University of Nottingham for use of the microscope and Linkam facilities.

**Appendix A**

The growth rate is assumed to be proportional to the absolute supersaturation of crystallisable components (which are lumped into a single pseudo-component)

$$\frac{dr}{dt} = k\left(c - c_f\right) \quad \text{(A.1)}$$

where c is concentration of crystallisable components in the liquid phase surrounding a crystal, and $c_f$ is the corresponding concentration at equilibrium (final concentration). The analysis can also be performed using a relative supersaturation driving force, i.e.

$$\frac{dr}{dt} = k' \frac{(c - c_f)}{c_f} \quad \text{(A.2)}$$

However, for isothermal experiments, $c_f$ can be regarded as a constant and so there is no practical difference between using the two expressions (apart from a differently defined kinetic constant *k'*).

As the crystal forms, the average concentration of crystallisable components in the surrounding liquid phase reduces. This can be quantified via a mass balance. It is assumed here that there is a fixed volume of liquid surrounding the crystal that contributes to the growth of the crystal and no other crystals*. This is assigned an initial radius R, and so for unit depth the volume of this liquid is $\pi R^2$. At any given time the total mass (M) of crystallisable components (liquid and solid) is given by,

$$M = \pi R^2 c + \pi r^2 c_s \quad \text{(A.3)}$$

Where *r* is the radius of the crystal and $c_s$ the overall concentration of crystallisable components within this radius (including trapped or entrained liquid).

At equilibrium, the equivalent expression is,

$$M = \pi R^2 c_f + \pi r_f^2 c_s \quad \text{(A.4)}$$

Where $r_f$ is the final crystal radius.

Equating the two masses (equations A.3 and A.4) gives,

$$\pi R^2 c + \pi r^2 c_s = \pi R^2 c_f + \pi r_f^2 c_s \quad \text{(A.5)}$$

Rearranging gives,

$$c - c_f = \frac{c_s\left(r_f^2 - r^2\right)}{R^2} \quad \text{(A.6)}$$

Insert into A.1, $$\frac{dr}{dt} = k\left(c - c_f\right) = \frac{kc_s\left(r_f^2 - r^2\right)}{R^2} \quad \text{(A.7)}$$

Rearrange, $$\frac{R^2}{\left(r_f^2 - r^2\right)} dr = kc_s dt \quad \text{(A.8)}$$

Integrate, $$\int_0^r \frac{R^2}{\left(r_f^2 - r^2\right)} dr = \int_{t_0}^t kc_s dt \quad \text{(A.9)}$$

$$\left[\frac{R^2}{r_f} \tanh^{-1}\left(\frac{r}{r_f}\right)\right]_0^r = [kc_s t]_{t_0}^t \quad \text{(A.10)}$$

$$\frac{R^2}{r_f} \tanh^{-1}\left(\frac{r}{r_f}\right) = kc_s(t - t_0) \quad \text{(A.11)}$$

Finally, $$\frac{r}{r_f} = \tanh\left(\frac{r_f}{R^2} kc_s(t - t_0)\right) \quad \text{(A.12)}$$

The general fit expression is therefore of the form

$$r = A \tanh\left(B(t - C)\right) \quad \text{(A.13)}$$

where $A = r_f$ , $B = \frac{r_f}{R^2} kc_s$ , $C = t_0$

The initial growth rate can be calculated via equation A.7 and setting r = 0, giving,

$$\left.\frac{dr}{dt}\right|_{r=0} = \frac{kc_s r_f^2}{R^2} = A\,B \quad \text{(A.14)}$$

Note that it is not possible to calculate the value of *k* from the fit parameters.

* The assumption of a constant volume of liquid associated with the growth of a crystal does not represent a true mass balance as the volume of this liquid will decrease as the crystallisable components are removed from it. It is possible to perform a “true” mass balance whereby the total system volume (solid crystal plus liquid that feeds it, i.e. $\pi R^2 + \pi r_f^2$) is conserved. A similar derivation method to the above yields the following expression:

$$t = \frac{r}{kc_s} + \frac{\left(R^2 - r_f^2\right)}{kc_s r_f} \tanh^{-1}\left(\frac{r}{r_f}\right) \quad \text{(A.15)}$$

This expression therefore requires the data to be plotted as t vs r. However, it is very difficult to perform fits with this equation due to the presence of the singularity in the $\tanh^{-1}$ function at $r = r_f$. For this reason equation A.15 was not used.

**References**

[1] R.E. Timms, Fractional crystallisation - the fat modification process for the 21st century, Eur. J. Lipid Sci. Technol., 107 (2005) 48-57.

[2] K. Kawamura, DSC Thermal-Analysis of Crystallisation Behavior in Palm Oil, J. Am. Oil Chem. Soc., 56 (1979) 753-758.

[3] K. Kawamura, DSC Thermal-Analysis of Crystallisation Behavior in Palm Oil, 2., J. Am. Oil Chem. Soc., 57 (1980) 48-51.

[4] W.L. Ng, C.H. Oh, A Kinetic-Study on Isothermal Crystallisation of Palm Oil by Solid Fat-Content Measurements, J. Am. Oil Chem. Soc., 71 (1994) 1135-1139.

[5] W.L. Ng, A Study of the Kinetics of Nucleation in a Palm Oil Melt, J. Am. Oil Chem. Soc., 67 (1990) 879-882.

[6] Ü. Riiner, Investigation of the Polymorphism of Fats and Oils by Temperature Programmed X-Ray Diffractometry, Lebensmittel -Wissenschaft und -Technologie, 3 (1970) 101-106.

[7] O. Zaliha, C.L. Chong, C.S. Cheow, A.R. Norizzah, M.J. Kellens, Crystallisation properties of palm oil by dry fractionation, Food Chem., 86 (2004) 245-250.

[8] U. Persmark, K.A. Melin, P.O. Stahl, Palm oil, its polymorphism and solidification properties, Riv. Ital. Sostanze Grasse, 53 (1976) 301-306.

[9] C.L. Chong, Z. Kamarudin, P. Lesieur, A. Marangoni, C. Bourgaux, M. Ollivon, Thermal and structural behaviour of crude palm oil: Crystallisation at very slow cooling rate, Eur. J. Lipid Sci. Technol., 109 (2007) 410-421.

[10] C.W. Chen, O.M. Lai, H.M. Ghazali, C.L. Chong, Isothermal Crystallisation Kinetics of Refined Palm Oil, J. Am. Oil Chem. Soc., 79 (2002) 403-410.

[11] C. Himawan, V.M. Starov, A.G.F. Stapley, Thermodynamic and Kinetic Aspects of Fat Crystallisation, Adv. Colloid Interface Sci., 122 (2006) 3-33.

[12] A.G.F. Stapley, C. Himawan, W. MacNaughtan, T.J. Foster, A Computational Method for Extracting Crystallisation Growth and Nucleation Rate Data from Hot Stage Microscope Images, Crystal Growth & Design, 9 (2009) 5061-5068.

[13] W.W. Christie, Chromatographic analysis of lipids : general principles, in: Lipid Analysis : Isolation, separation, identification and structural analysis of lipids, The Oily Press, an imprint of PJ Barnes and Associates, Bridgewater, UK, 2003.

**Figure captions**

Figure 1. Images showing sequence of events in algorithm to identify newly appeared nuclei: (a) map showing “new” pixels, (b) result of transformation whereby the number of non-zero pixels within a square surrounding each pixel position is returned at that pixel, and (c) results of subsequent thresholding which is used to identify the existence and position of a new nucleus. The example is taken from a section of an image during crystallisation at 30 °C. The image dimensions correspond to 120 x 120 microns.

Figure 2. Example of final microscope image and associated crystalmaps obtained from the isothermal crystallisation of palm oil at 29 °C – (a) original image in grayscale (with increased contrast), (b) base crystalmap that is built up over time, (c) crystalmap with “holes filled”, (d) “cleaner” version of the unfilled crystalmap (Figure 2b) that more closely represents the original image, (e) original image showing circles indicating calculated radii of crystals (radii of crystals near the edge of the image are not calculated). Dimensions on each image correspond to 745 x 596 microns.

Figure 3. Images showing crystal morphology after holding at various isothermal hold temperatures: (a) 20 °C, (b) 22 °C, (c) 24 °C, (d) 26 °C, (e) 28 °C, (f) 30 °C, (g) 32 °C, (h) 35 °C. All images represent 120 x 120 microns.

Figure 4. Images showing changes in crystal morphology at the following times during isothermal crystallisation at 24 °C: (a) 10 min, (b) 20 min and (c) 30 min; and then followed by warming at 1 °C/min to (d) 36 °C, (e) 39 °C, (f) 42 °C, (g) 45 °C and (h) 47 °C. All images represent 120 x 120 microns.

Figure 5. Fractional coverage (solid fat content) vs time during the isothermal crystallisation of palm oil at various temperatures: (a) from “filled” crystalmaps and (b) from “unfilled” crystalmaps.

Figure 6. Number of crystals vs time during the isothermal crystallisation of palm oil at various temperatures: (a) vs t and (b) vs $t_{mod}$.

Figure 7. Nucleation rate vs temperature calculated (a) per unit volume of visible sample, (b) per unit area of visible sample.

Figure 8. Calculated radii vs time for crystal growth at (a) 23 °C, (b) 26 °C, (c) 29 °C, and (d) 32 °C.

Figure 9. Fits of representative curves at each temperature to linear (over first part of each curve, dot-dash line), tanh (solid line) and exponential expressions (dashed line), for (a) 23 °C (example “early” and “late” curves), 24 °C, 25 °C, 26 °C, and (b) 27 °C, 28 °C, 29 °C, 30 °C and 32 °C.

Figure 10. Growth rates vs temperature obtained from different fit methods. Error bars show standard deviations based on different crystals analysed.

Figure 11. Final cumulative crystal size distribution at each temperature. The radial values used for each crystal correspond to a circle of the same area of the crystal.

Table 1 – Composition of RBD palm oil as determined by HPLC (where O = oleic, L = linoleic, M = myristic, P = palmitic and S = stearic acids).

| Component | Area % |
|---|---|
| Others | 5.29 |
| OLL | 0.39 |
| PLL | 2.27 |
| MLP | 0.54 |
| OOL | 2.00 |
| POL | 10.54 |
| PLP | 9.35 |
| MPP | 0.44 |
| OOO | 4.25 |
| POO | 23.87 |
| POP | 28.26 |
| PPP | 4.79 |
| SOO | 2.31 |
| POS | 4.36 |
| PPS | 0.87 |
| SOS | 0.48 |

Table 2 – Summary of induction time, nucleation rate, initial growth rate and final melting data for each isothermal hold temperature. Growth rates are given as average ± standard deviation based on all crystals which grow above 15 μm in size, with average RMS error values (in μm) shown below in brackets.

| Temperature (°C) | Induction time (s) | Nucleation rate per unit | | | Average initial growth rate (μm $s^{-1}$) | | | | Final melting temperature (°C) |
|---|---|---|---|---|---|---|---|---|---|
| | | area, this study ($mm^{-2}$ $s^{-1}$) | volume, this study ($mm^{-3}$ $s^{-1}$) | volume, literature[2] ($mm^{-3}$ $s^{-1}$) | This study, linear fit over first 30% of growth | This study, tanh fit | This study, exp fit | Literature[2] | |
| 23 | 45 ± 15 | 1.09 | 91.43 | | 0.0615 ± 0.0179 (0.317 μm) | 0.0301 ± 0.0112 (0.285 μm) | 0.0401 ± 0.0121 (0.304 μm) | | 47 |
| 24 | 105 ± 15 | 0.52 | 44.06 | | 0.0248 ± 0.060 (0.274 μm) | 0.0262 ± 0.0045 (0.471 μm) | 0.0335 ± 0.0064 (0.337 μm) | | 42*, 47† |
| 25 | 195 ± 15 | 0.33 | 61.79 | | 0.0211 ± 0.0098 (0.254 μm) | 0.0308 ± 0.0046 (0.339 μm) | 0.0432 ± 0.0082 (0.469 μm) | | 42*, 47† |
| 26 | 375 ± 15 | 0.72 | 4.59 | 0.400 | 0.0274 ± 0.0042 (0.313 μm) | 0.0329 ± 0.0054 (0.552 μm) | 0.0450 ± 0.0095 (1.088 μm) | 0.055 | 44 |
| 27 | 525 ± 15 | 0.116 | 9.78 | | 0.0295 ± 0.0058 (0.278 μm) | 0.0361 ± 0.0058 (0.361 μm) | 0.0479 ± 0.0081 (0.854 μm) | | 44 |
| 28 | 585 ± 15 | 0.037 | 7.79 | 0.267 | 0.0256 ± 0.0081 (0.259 μm) | 0.0293 ± 0.0071 (0.508 μm) | 0.0284 ± 0.0048 (2.372 μm) | 0.052 | 45 |
| 29 | 1095 ± 15 | 0.034 | 2.82 | | 0.0253 ± 0.0079 (0.378 μm) | 0.0297 ± 0.0061 (0.319 μm) | 0.0376 ± 0.0098 (1.248 μm) | | 45 |
| 30 | 1710 ± 30 | 0.028 | 2.33 | 0.217 | 0.0279 ± 0.0082 (0.358 μm) | 0.0309 ± 0.0072 (0.458 μm) | 0.0418 ± 0.0133 (4.383 μm) | 0.045 | 46 |
| 32 | 1350 ± 30 | 0.0015 | 0.32 | | 0.0144 ± 0.0008 (0.265 μm) | 0.0115 ± 0.0007 (0.358 μm) | 0.0150 ± 0.0010 (0.148 μm) | 0.040 | 47 |

* refers to the outer regions of crystals (see Figure 4). † refers to the core of crystals

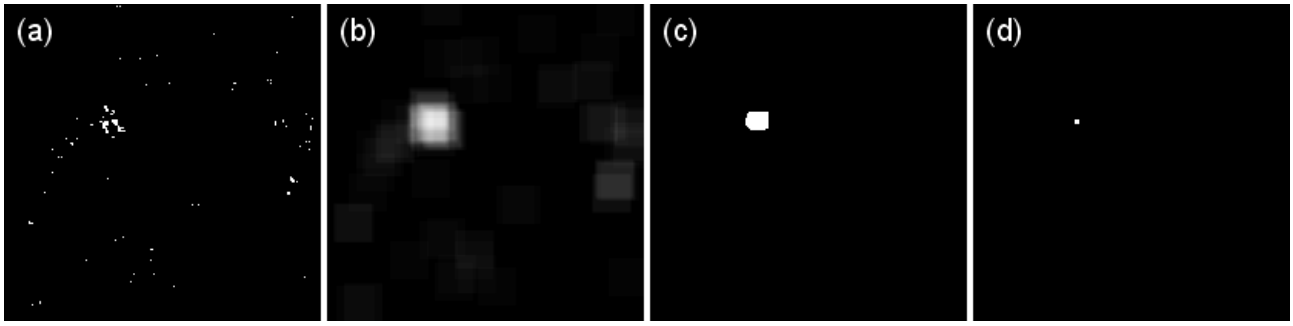


Figure 1. Images showing sequence of events in algorithm to identify newly appeared nuclei: (a) map showing “new” pixels, (b) result of transformation whereby the number of non-zero pixels within a square surrounding each pixel position is returned at that pixel, and (c) results of subsequent thresholding which is used to identify the existence and position of a new nucleus. The example is taken from a section of an image during crystallisation at 30 °C. The image dimensions correspond to 120 x 120 microns.

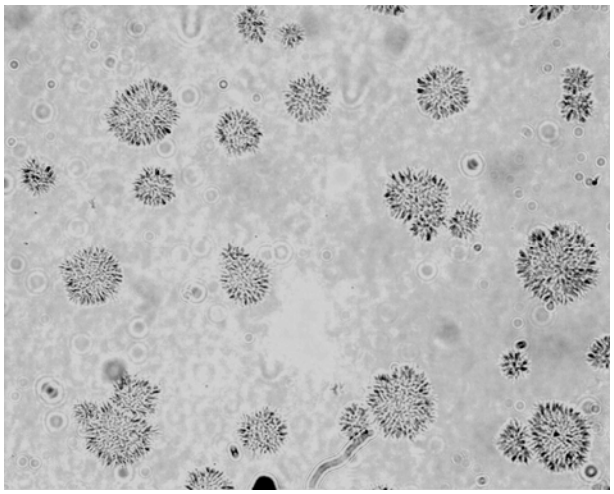

(a)

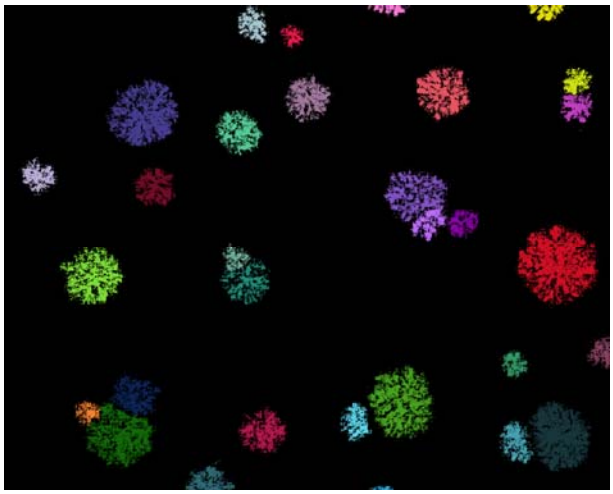

(b)

(c)

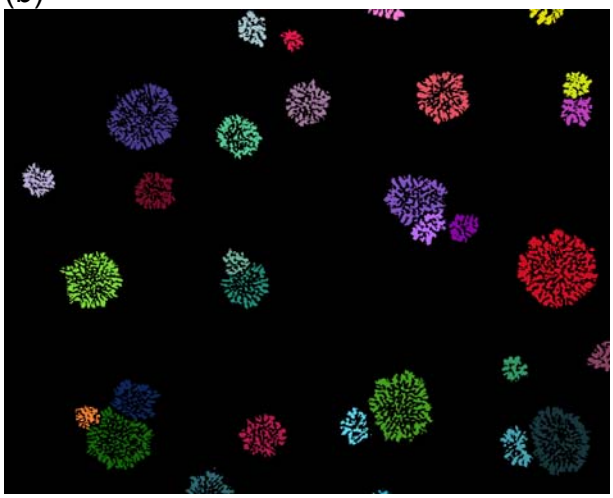

(d)

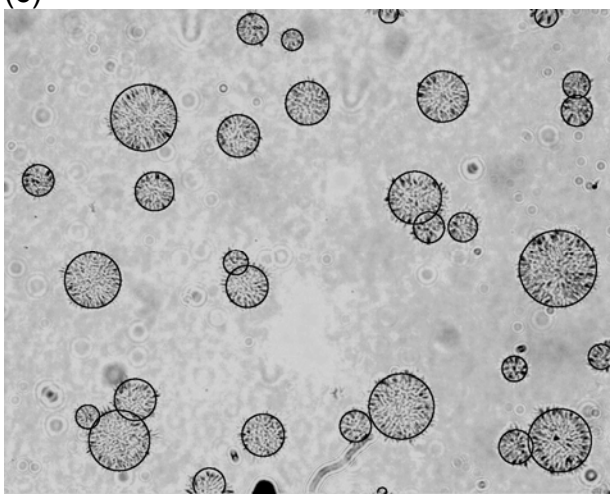

(e)

Figure 2. Example of final microscope image and associated crystalmaps obtained from the isothermal crystallisation of palm oil at 29 °C – (a) original image in grayscale (with increased contrast), (b) base crystalmap that is built up over time, (c) crystalmap with "holes filled", (d) "cleaner" version of the unfilled crystalmap (Figure 2b) that more closely represents the original image, (e) original image showing circles indicating calculated radii of crystals (radii of crystals near the edge of the image are not calculated). Dimensions on each image correspond to 745 x 596 microns.

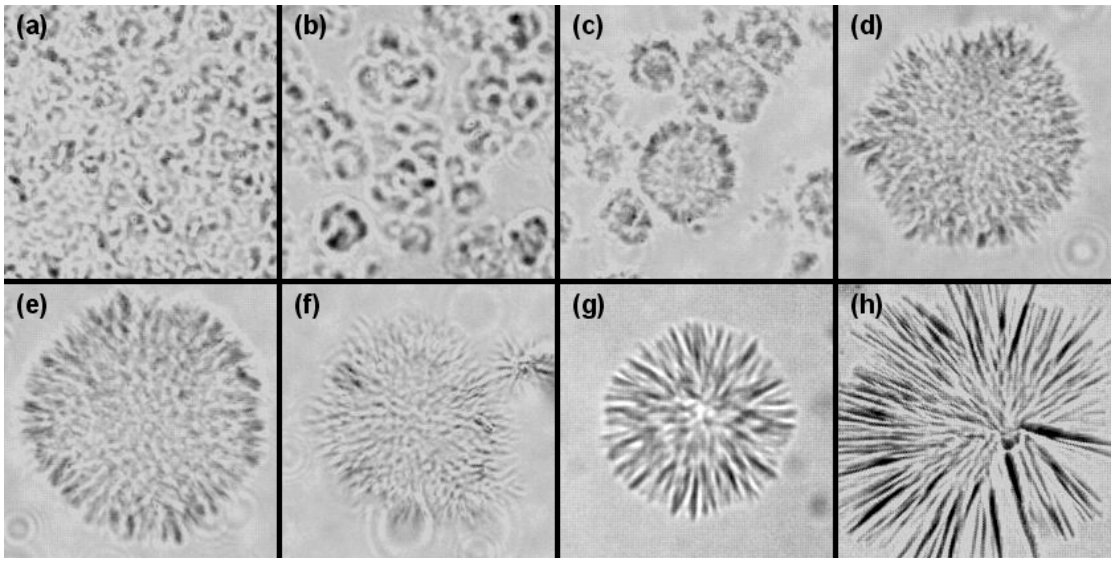


Figure 3. Images showing crystal morphology after holding at various isothermal hold temperatures: (a) 20 °C, (b) 22 °C, (c) 24 °C, (d) 26 °C, (e) 28 °C, (f) 30 °C, (g) 32 °C, (h) 35 °C. All images represent 120 x 120 microns.

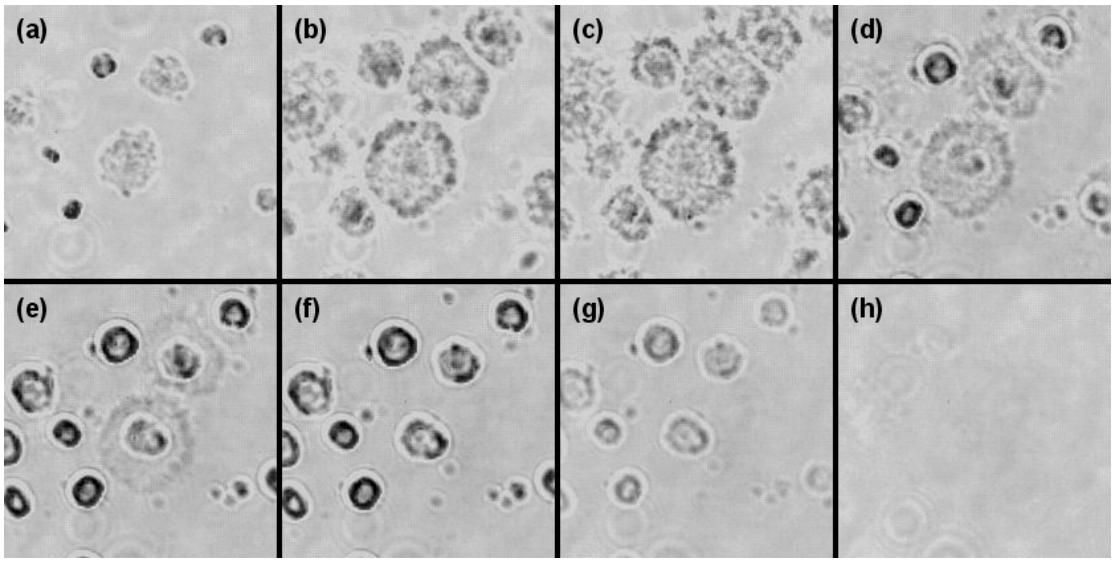


Figure 4. Images showing changes in crystal morphology at the following times during isothermal crystallisation at 24 °C: (a) 10 min, (b) 20 min and (c) 30 min; and then followed by warming at 1 °C/min to (d) 36 °C, (e) 39 °C, (f) 42 °C, (g) 45 °C and (h) 47 °C. All images represent 120 x 120 microns.

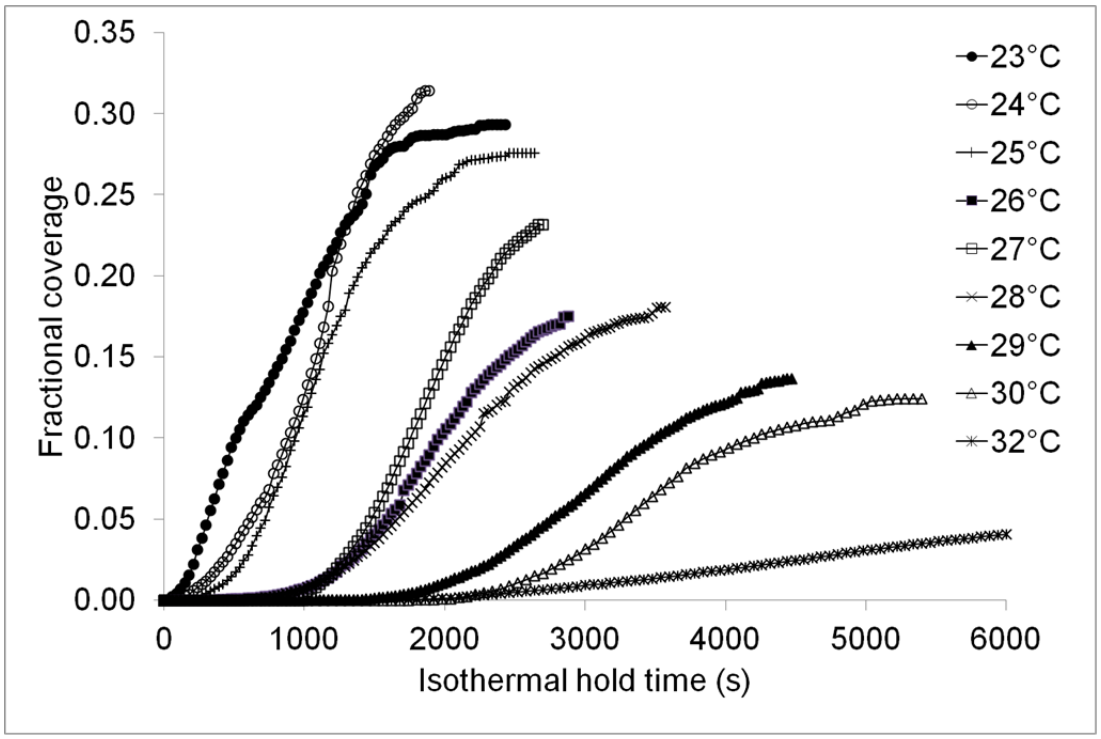


(a)

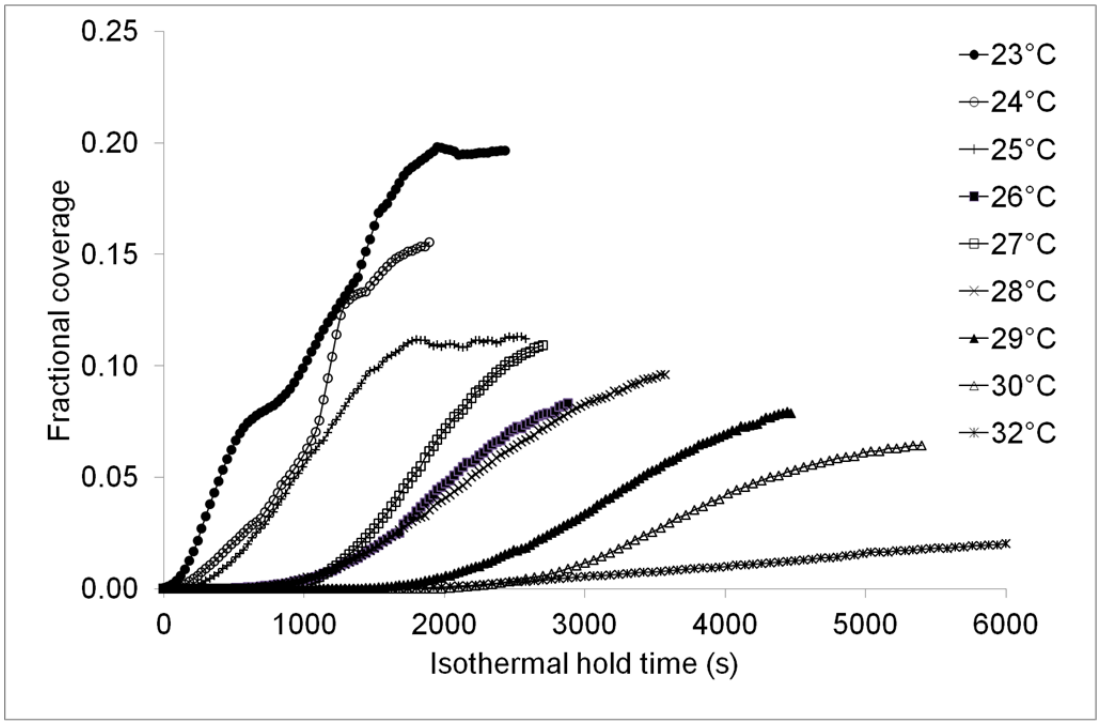


(b)

Figure 5. Fractional coverage (solid fat content) vs time during the isothermal crystallisation of palm oil at various temperatures: (a) from “filled” crystalmaps and (b) from “unfilled” crystalmaps.

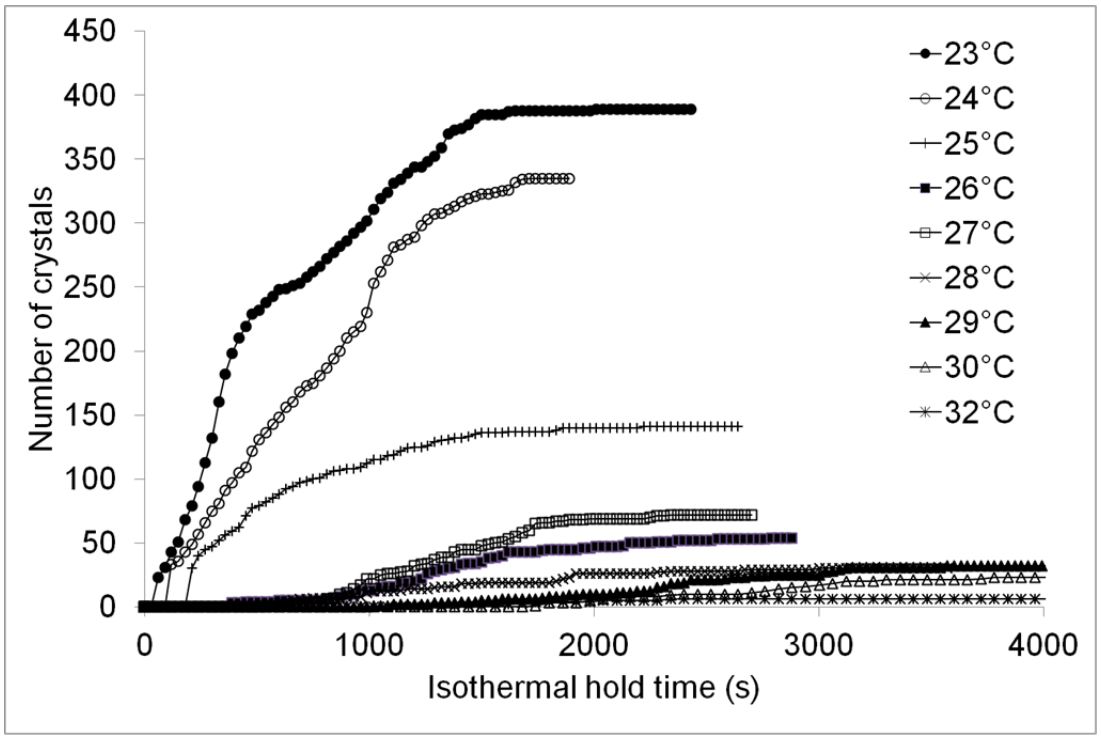


(a)

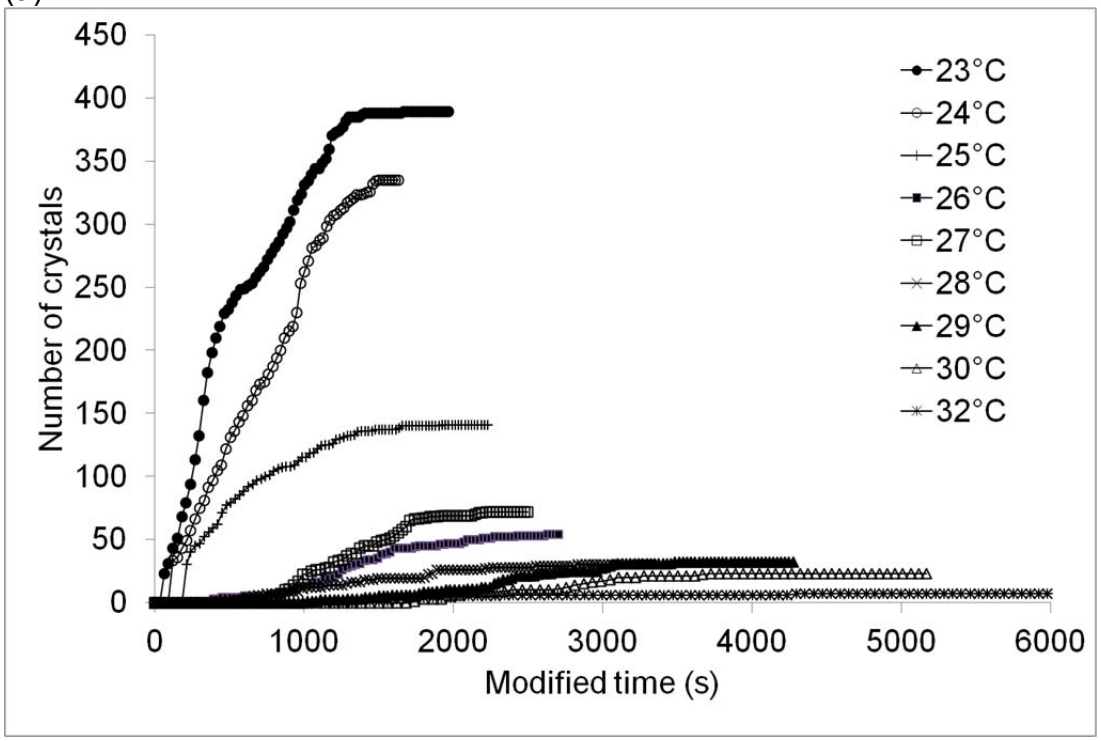


(b)

Figure 6. Number of crystals vs time during the isothermal crystallisation of palm oil at various temperatures: (a) vs t and (b) vs $t_{mod}$.

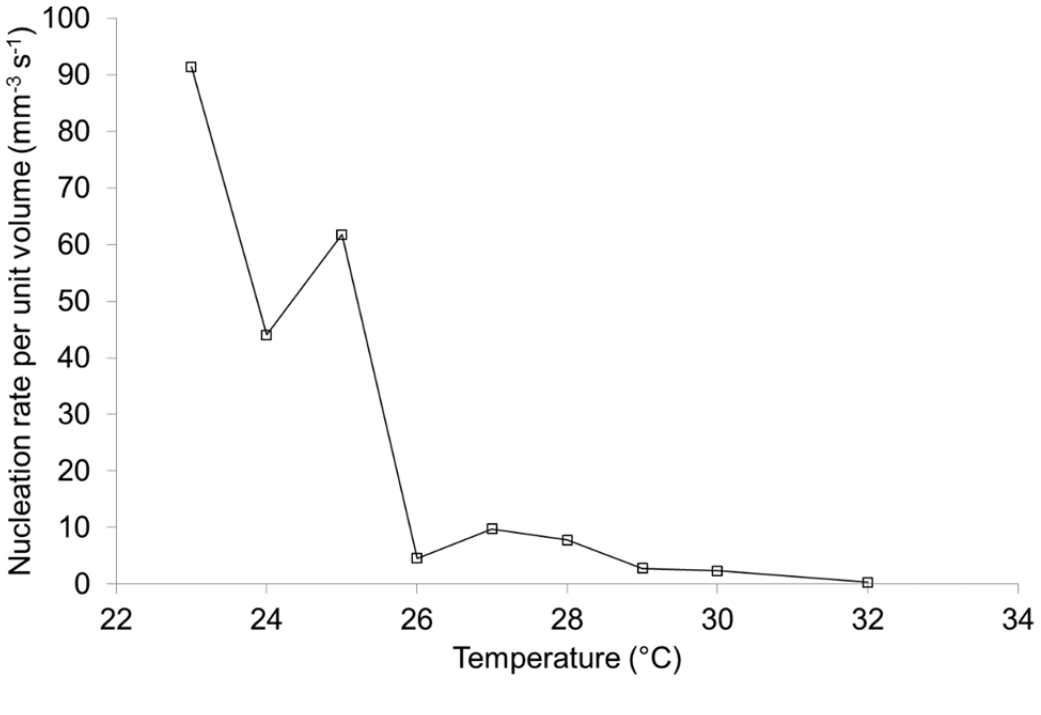


(a)

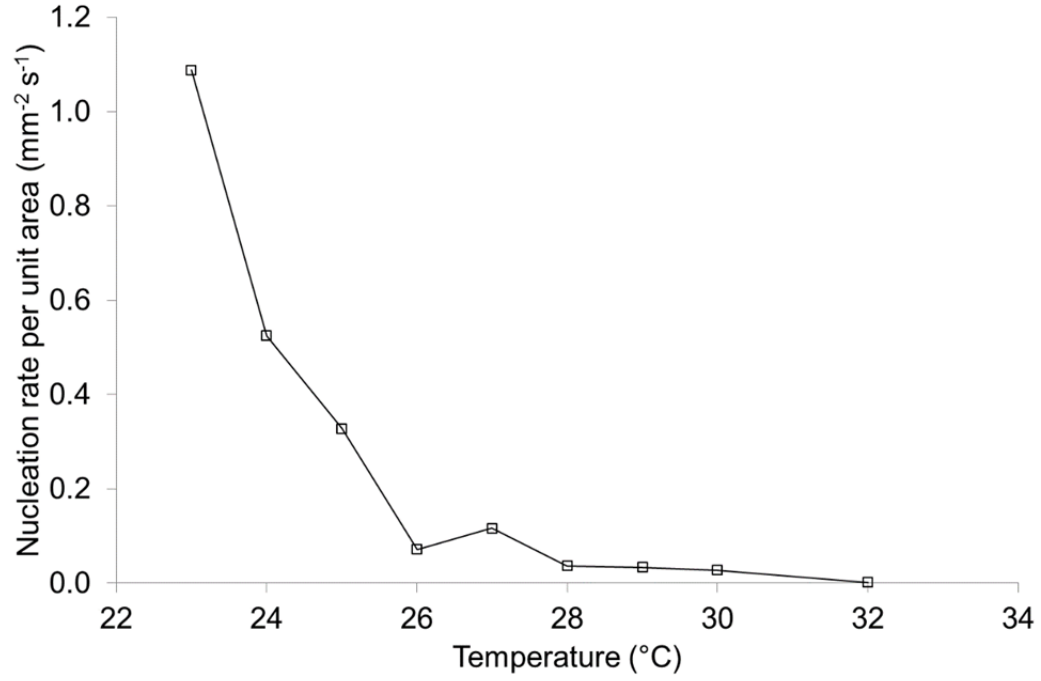


(b)

Figure 7. Nucleation rate vs temperature calculated (a) per unit volume of visible sample, (b) per unit area of visible sample.

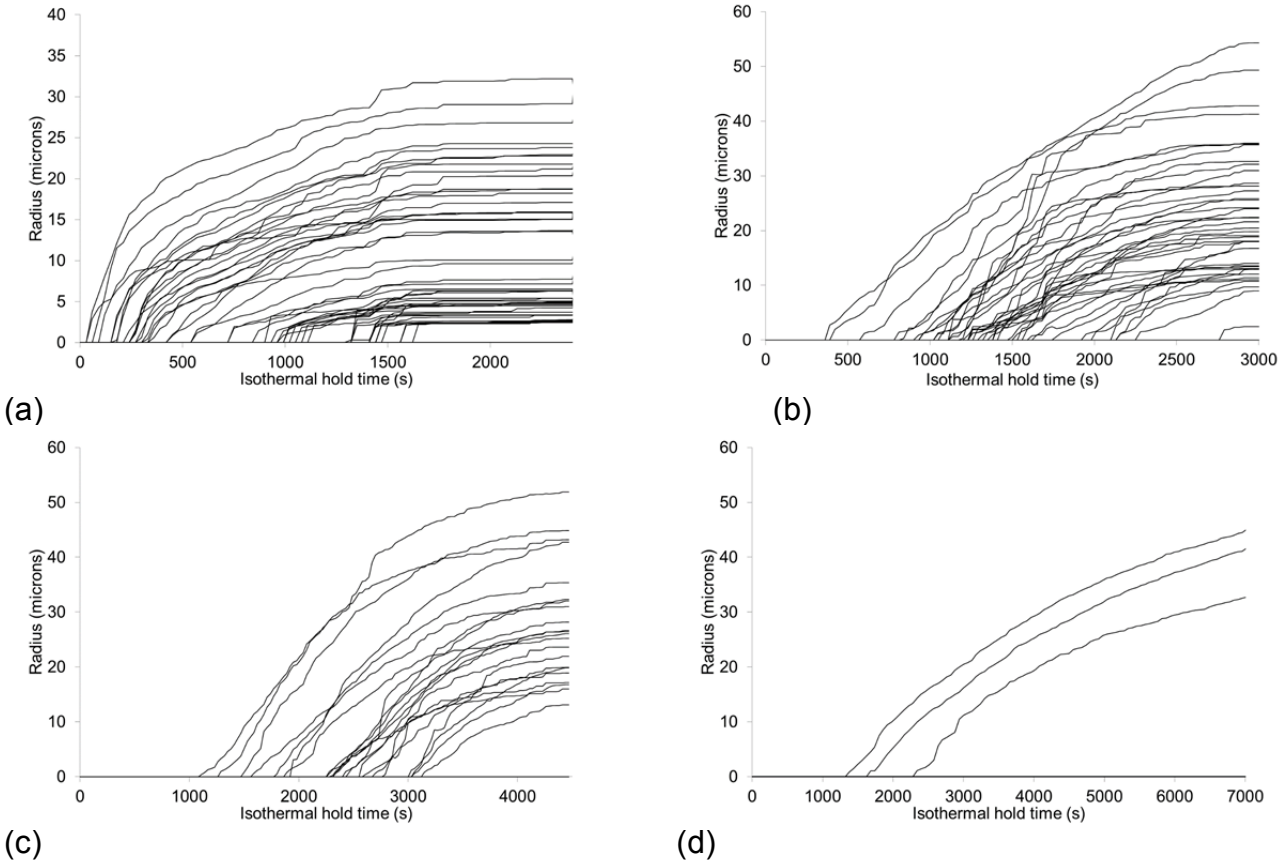


Figure 8. Calculated radii vs time for crystal growth at (a) 23 °C, (b) 26 °C, (c) 29 °C, and (d) 32 °C.

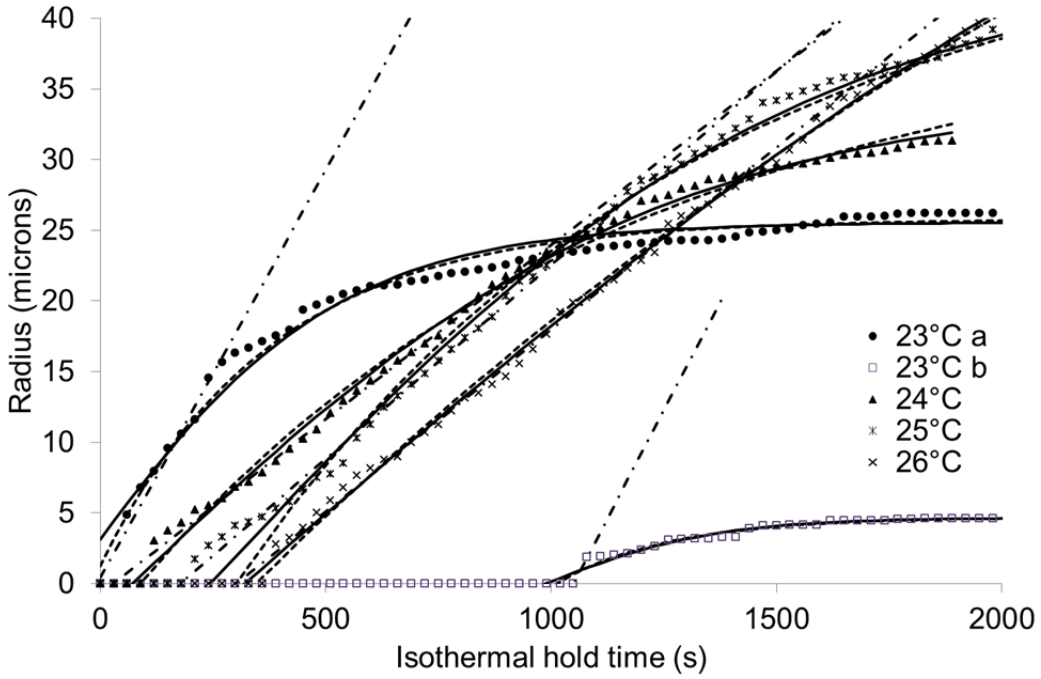


(a)

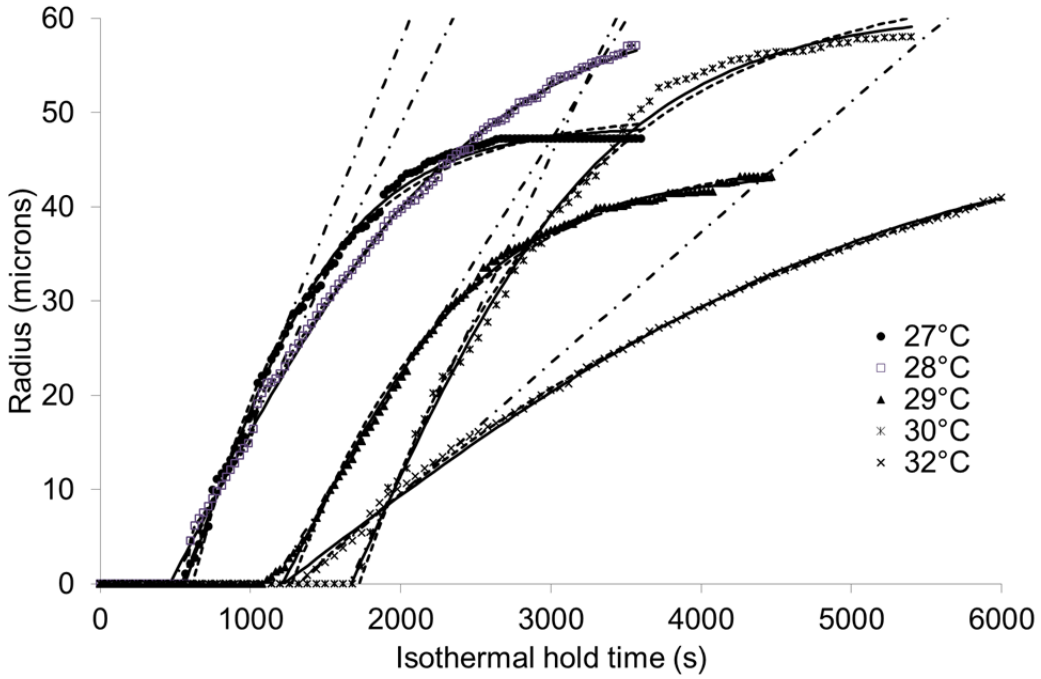


(b)

Figure 9. Fits of representative curves at each temperature to linear (over first part of each curve, dot-dash line), tanh (solid line) and exponential expressions (dashed line), for (a) 23 °C (example “early” and “late” curves), 24 °C, 25 °C, 26 °C, and (b) 27 °C, 28 °C, 29 °C, 30 °C and 32 °C.

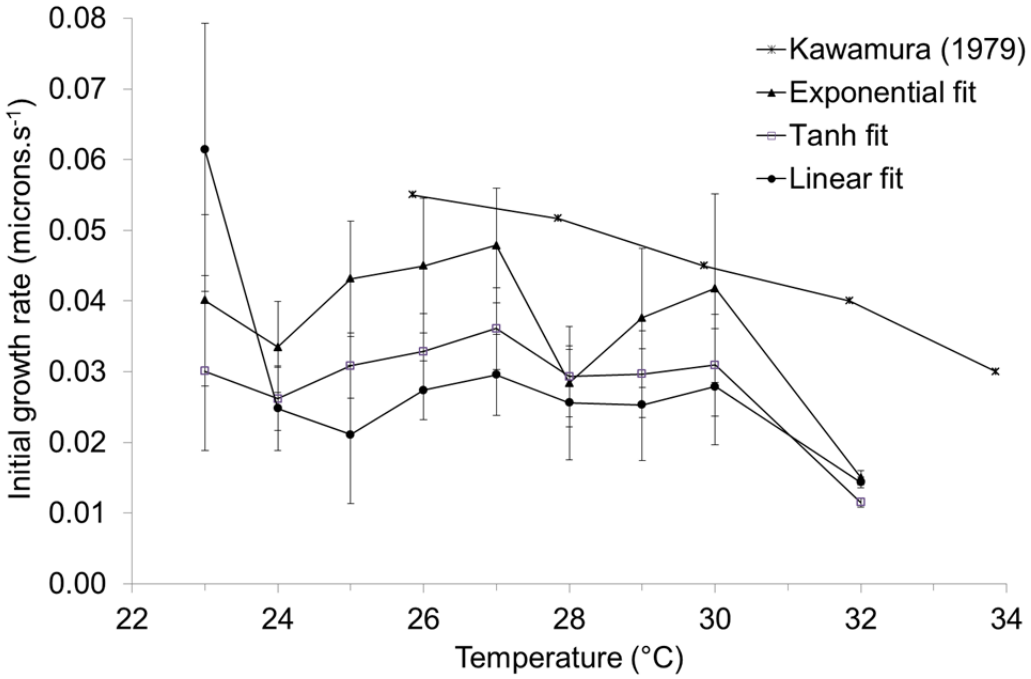


Figure 10. Growth rates vs temperature obtained from different fit methods. Error bars show standard deviations based on different crystals analysed.

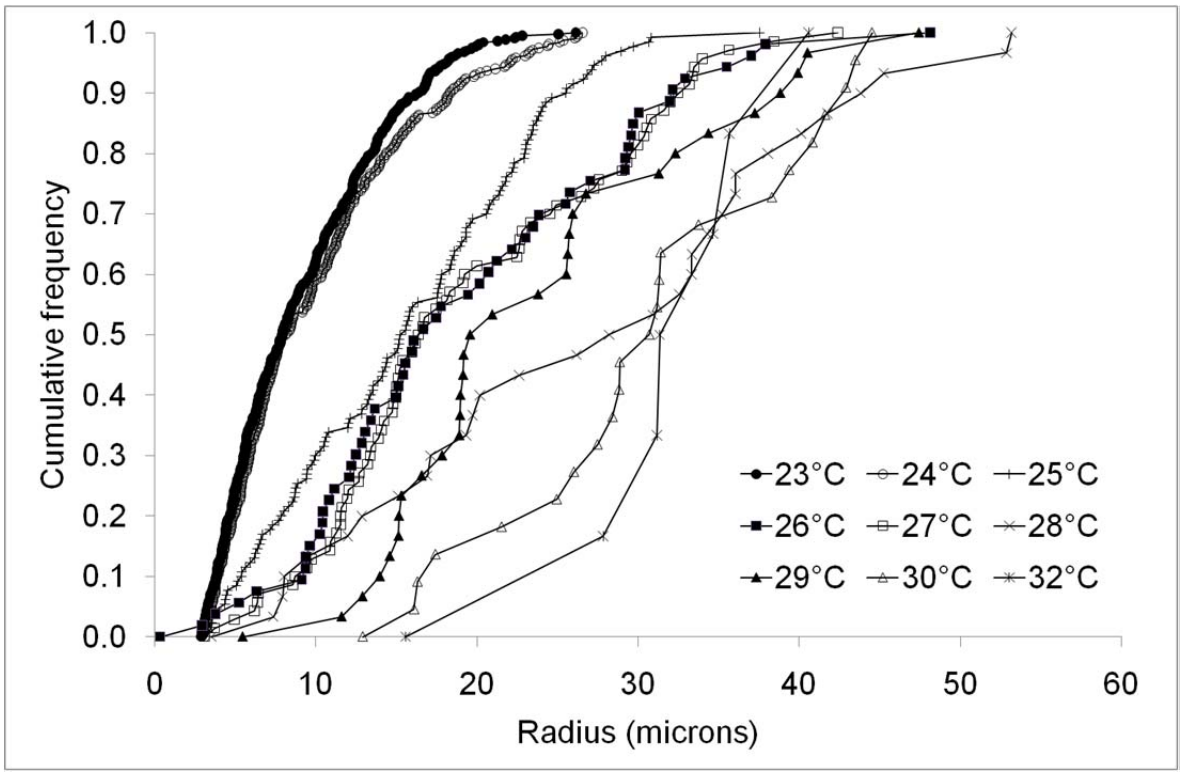


Figure 11. Final cumulative crystal size distribution at each temperature. The radial values used for each crystal correspond to a circle of the same area of the crystal.